

First exploration of wobbling modes in an isotone chain: The $N = 59$ caseH. M. Dai , Q. B. Chen ,* and Xian-Rong Zhou*Department of Physics, East China Normal University, Shanghai 200241, China* (Received 2 July 2023; revised 8 October 2023; accepted 23 October 2023; published 14 November 2023)

The possible existence of wobbling modes in the $N = 59$ isotones ^{95}Kr , ^{97}Sr , ^{99}Zr , ^{101}Mo , ^{103}Ru , ^{105}Pd , and ^{107}Cd is explored by the constrained triaxial covariant density functional theory combined with quantum particle rotor model calculations. It is found that there are several states with suitable triaxial deformations and high- j particle configuration to establish wobbling modes in ^{97}Sr , ^{99}Zr , ^{101}Mo , ^{103}Ru , and ^{105}Pd . The available experimental energy spectra based on the $\nu(1h_{11/2})^1$ configuration in ^{97}Sr and ^{99}Zr are described well. The decreased energy difference between the doublet bands, the enhanced $B(E2)_{\text{out}}/B(E2)_{\text{in}}$ values, as well as the one-phonon oscillation characteristic of the total angular momentum indicate that the two nuclei can be transverse wobbling candidates, which suggests the possibility of a larger region of wobbling modes near the $A \approx 100$ mass region.

DOI: [10.1103/PhysRevC.108.054306](https://doi.org/10.1103/PhysRevC.108.054306)**I. INTRODUCTION**

Wobbling motion was first predicted for a nucleus with stable triaxial deformation by Bohr and Mottelson in the 1970s [1]. For a triaxially deformed nucleus, the moments of inertia of the three principal axes are not equal to each other. Although the triaxial nucleus favors rotation around the principal axis with the largest moment of inertia to minimize the energy, the rotation around the other two principal axes will affect the principal axis rotation, and as a result the rotation axis of the nucleus deviates from the principal axis, resulting in the wobbling motion of the nucleus [1].

When the triaxial rotor is coupled with a high- j valence particle, Frauendorf and Dönau pointed out that there are two different wobbling modes, namely, longitudinal wobbling (LW) and transverse wobbling (TW) [2]. The longitudinal wobbling means that the angular momentum of the high- j valence particles is parallel to the principal axis with the largest moment of inertia, while the transverse wobble means that the angular momentum of the high- j valence particles is perpendicular to the principal axis with the largest moment of inertia. In Ref. [3], Chen and Frauendorf further proposed a more comprehensive classification for the wobbling motion based on the topology of the classical orbits visualized by the corresponding spin coherent state (SCS) maps: LW corresponds to a revolution of total angular momentum J around the axis with the largest moment of inertia and TW corresponds to a revolution of J around an axis perpendicular to the axis with the largest moment of inertia. The salient experimental criteria for TW and LW are manifested on the excitation energy and the $E2$ transition. The excitation energy of the LW (TW) states increases (decreases) with increasing angular momentum. Both TW and LW have enhanced $I \rightarrow I - 1$ $E2$ transitions between adjacent wobbling bands.

The wobbling motion was initially predicted in even-even nuclei without the valence quasiparticles, but the experimental evidence for this is still fragmentary. The only candidates observed experimentally up to now are ^{112}Ru [4] and ^{114}Pd [5], in which the γ bands are interpreted as a combination of $n = 1$ (odd-spin) and $n = 2$ (even-spin) wobbling excitations as the odd-even staggering pattern agrees with the expectation of rigid triaxiality. However, no electromagnetic transition data were reported to put the wobbling interpretation on solid ground.

In contrast, solid evidence of the wobbling motion signal was reported for the first time in the $A \approx 160$ mass region ^{163}Lu in 2001 for the one-phonon wobbling excitation [6] and in 2002 for the two-phonon wobbling excitation [7]. Later on, studies were carried out in the nearby nuclei, including ^{161}Lu [8], ^{165}Lu [9], ^{167}Lu [10], ^{167}Ta [11], and the latest ^{151}Eu [12], in which the wobbling bands are built on the configuration $\pi i_{13/2}$ (except for ^{151}Eu [12] built on $\pi h_{11/2}$). After proposing the concepts of LW and TW [2], experimental evidence of wobbling motion has also been reported in other mass regions. In detail, in the $A \approx 130$ mass region there are candidates ^{135}Pr [13,14], ^{133}La [15], ^{130}Ba [16–18], ^{127}Xe [19], ^{133}Ba [20], and ^{136}Nd [21], of which ^{135}Pr provided the first observation of transverse wobbling at low deformation [13,14] and ^{130}Ba the first example of two-quasiparticle wobbling bands in an even-even nucleus [17,18]. In the $A \approx 190$ mass region, two candidates ^{187}Au [22] and ^{183}Au [23] were reported. The ^{187}Au result is the first experimental evidence of longitudinal wobbling bands where the expected signature partner band has also been identified [22], and the ^{183}Au result is the first observation of multiple transverse wobbling bands of different kinds [23]. However, one notes that some of these suggested wobblers remain controversial [24–31]. In the $A \approx 100$ mass region, there is only one candidate, ^{105}Pd , with odd neutron number $N = 59$, which had been suggested as TW and is the first nucleus in which the wobbling excited state is based on a quasineutron configuration [32]. Although only one wobbling

*Corresponding author: qbchen@phy.ecnu.edu.cn

candidate was reported in the $A \approx 100$ mass region, much evidence of nuclear chiral doublet bands or multiple chiral doublet bands has been reported (see, e.g., Refs. [33–37]), which indicates that the $A \approx 100$ mass region is a typical triaxially deformed region. It is therefore very interesting to investigate whether there are more wobbling nuclei in the $A \approx 100$ mass region, in particular among the $N = 59$ isotones.

It is known that there are two necessary conditions for establishing the wobbling mode, i.e., significant triaxial deformation and high- j particle(s) or hole(s) configuration. The triaxial deformation determines whether or not the wobbling mode exists [1], while the configuration determines the classification of the wobbling mode [2,3]. Qualitatively, a triaxially deformed configuration with particles at the bottom of the deformed j shell or holes at the top of the shell gives a TW mode, while a configuration with quasiparticles located at the middle of the shell gives a LW mode. Therefore, to search for the wobbling candidates in the $A \approx 100$ mass region, a reliable theoretical approach is needed to get the information of the configuration and deformation for a specific nucleus. The covariant density functional theory (CDFT) provides such a tool. The CDFT, based on the mean field approach, has played an important role in a fully microscopic and universal description for a large number of nuclear phenomena [38–42]. In particular, the adiabatic and configuration fixed constrained triaxial CDFT has been developed [43] and used widely [44–49] to study the possible configurations and the corresponding deformations in nuclei to search for the possible existence of the nuclear chirality or multiple chirality, another fingerprint of triaxiality or triaxiality coexistence [43,50]. In fact, the adiabatic and configuration fixed constrained triaxial CDFT has been already extended successfully to describe the wobbling candidates reported in ^{105}Pd [32], ^{130}Ba [17], ^{187}Au [22], and ^{183}Au [23] as well as to predict the possible existence of wobbling modes in $A \approx 60$ mass region nuclei [51].

In this work, we will use the constrained CDFT to study the configurations and the triaxial deformations for the $N = 59$ isotones in the $A \approx 100$ mass region, viz., ^{95}Kr ($Z = 36$), ^{97}Sr ($Z = 38$), ^{99}Zr ($Z = 40$), ^{101}Mo ($Z = 42$), ^{103}Ru ($Z = 44$), ^{105}Pd ($Z = 46$), and ^{107}Cd ($Z = 48$), to search for the possible existence of wobbling modes. The aim of this study is to provide a theoretical information for the forthcoming experimental investigations on triaxial deformation and wobbling motion in $N = 59$ isotones.

II. RESULTS AND DISCUSSION

First, we will carry out the adiabatic and configuration fixed constrained triaxial CDFT calculations to obtain the potential energy surfaces (PESs) in the β - γ plane to learn the ground state properties for the isotones ^{95}Kr , ^{97}Sr , ^{99}Zr , ^{101}Mo , ^{103}Ru , ^{105}Pd , and ^{107}Cd . Subsequently, the single-particle energy levels, deformation parameters (β , γ), as well as the potential energy curves (PECs) will be used to analyze the possible configurations and deformations to search for the possible existence of wobbling motions. Finally, ^{97}Sr and ^{99}Zr based on the $\nu(1h_{11/2})^1$ configuration are used as examples to show the possible wobbling evidence, employing the quantal

particle rotor model (PRM) [3,17,52–54] and the harmonic frozen alignment (HFA) approximation [2].

A. Covariant density functional theory results

The detailed formalism and numerical techniques of the adiabatic and configuration fixed constrained CDFT calculation adopted in this work can be found in Ref. [43] and references therein. Here “adiabatic” means that the nucleons always occupy the lowest single particle levels during the constraint process, while “configuration fixed” means that the nucleons must occupy the same combination of the single-particle levels during the constraint process. In the present calculations, the point-coupling density functional PC-PK1 [55] is adopted, while the pairing correlations are neglected for simplicity. The Dirac equation is solved in a set of three-dimensional harmonic oscillator basis with 12 major oscillator shells.

In Fig. 1, the PESs of ^{95}Kr , ^{97}Sr , ^{99}Zr , ^{101}Mo , ^{103}Ru , ^{105}Pd , and ^{107}Cd are shown. They are obtained by simultaneously constraining the quadrupole moments q_{20} and q_{22} using the quadratic constraints function

$$\langle H \rangle + \frac{1}{2} \sum_{\mu=0,2} C_{2\mu} (\langle \hat{Q}_{2\mu} \rangle - q_{2\mu})^2, \quad (1)$$

where $\langle H \rangle$ is the total energy, $C_{2\mu}$ the constraint strength constants, and $\langle \hat{Q}_{2\mu} \rangle$ the expectation value of the mass quadrupole operator:

$$\hat{Q}_{20} = 2z^2 - x^2 - y^2, \quad \hat{Q}_{22} = x^2 - y^2. \quad (2)$$

The constrained values of $q_{2\mu}$ are related to the deformation parameters by

$$\beta = \frac{4\pi}{3AR_0^2} \sqrt{q_{20}^2 + 2q_{22}^2}, \quad \text{with } R_0 = 1.2A^{1/3} \text{ fm}, \quad (3)$$

$$\gamma = \arctan \frac{\sqrt{2}q_{22}}{q_{20}}. \quad (4)$$

The PESs are shown in a range of $\beta = 0$ – 0.6 and $\gamma = 0^\circ$ – 60° . The energy minimum, namely the ground state, is represented by a red star in the figure. The ground state of ^{95}Kr is located at ($\beta = 0.32$, $\gamma = 60^\circ$), which means that its shape is oblate. In ^{97}Sr , the ground state deformation is ($\beta = 0.49$, $\gamma = 0^\circ$), indicating that the nucleus does not have a triaxial deformation structure. Similarly, we can get the ground state information for the other nuclei. The corresponding deformation parameters for the ground states in ^{99}Zr , ^{101}Mo , ^{103}Ru , ^{105}Pd , and ^{107}Cd are ($\beta = 0.49$, $\gamma = 0^\circ$), ($\beta = 0.58$, $\gamma = 0^\circ$), ($\beta = 0.28$, $\gamma = 21.3^\circ$), ($\beta = 0.19$, $\gamma = 0^\circ$), and ($\beta = 0.18$, $\gamma = 4.9^\circ$), respectively. To sum up, only the nucleus ^{103}Ru has significant triaxial deformation among these nuclei.

Apart from the remarkable triaxial deformation, it is necessary to have a configuration with high- j particle(s) or hole(s) to establish the wobbling mode. To check the possible existence of the configuration along the $N = 59$ isotones, we present in Fig. 2 the single-particle energy levels of neutrons (left column) and protons (right column) near the Fermi surface for the ground state in ^{103}Ru as an example. One

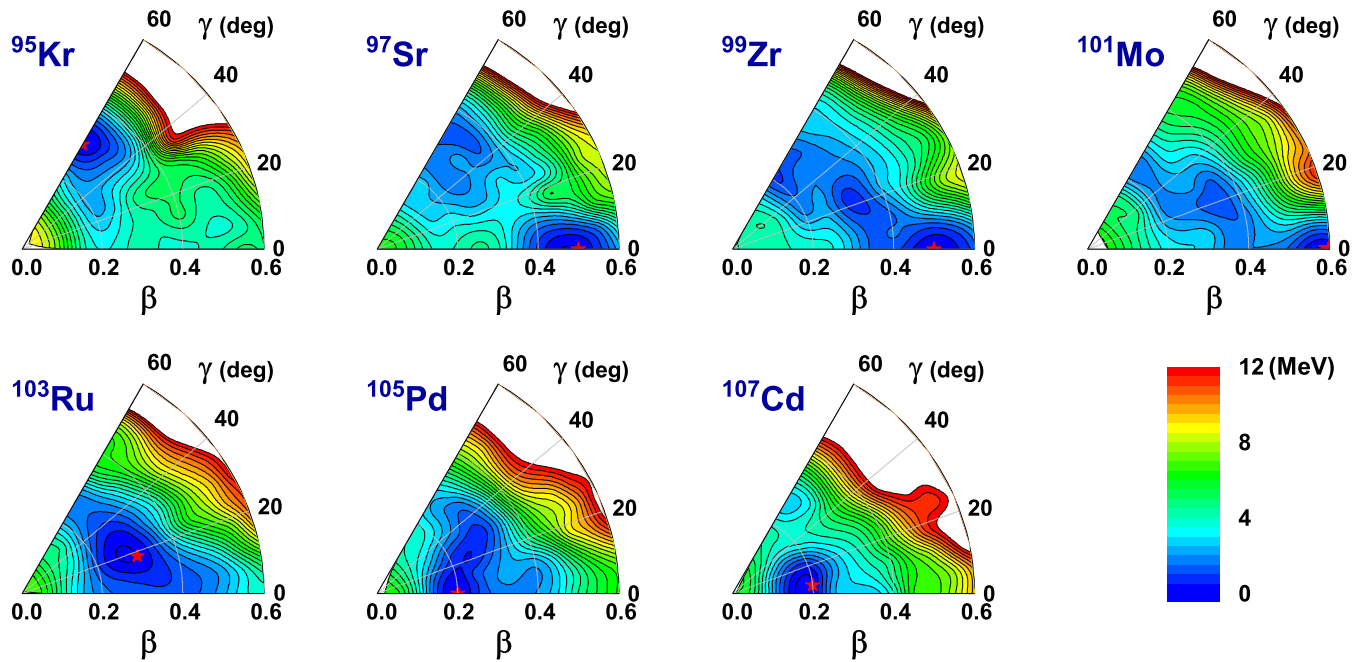


FIG. 1. Potential energy surfaces in the β - γ plane for ^{95}Kr , ^{97}Sr , ^{99}Zr , ^{101}Mo , ^{103}Ru , ^{105}Pd , and ^{107}Cd obtained by constrained CDFT calculations. All energies are normalized with respect to the binding energy of the absolute minimum (red star). The energy separation between each contour line is 0.5 MeV.

sees that there is a large energy gap at the neutron number 54 and the proton number 40, and the corresponding single-particle occupation can be seen clearly as well. The neutron Fermi surface is located at the $h_{11/2}$ orbital. Accordingly, the corresponding configuration of the ground state in ^{103}Ru is $\pi(1g_{9/2})^6 \otimes \nu(1g_{7/2})^6(2d_{5/2})^2(1h_{11/2})^1$, which satisfies the condition of the configuration with a high- j particle.

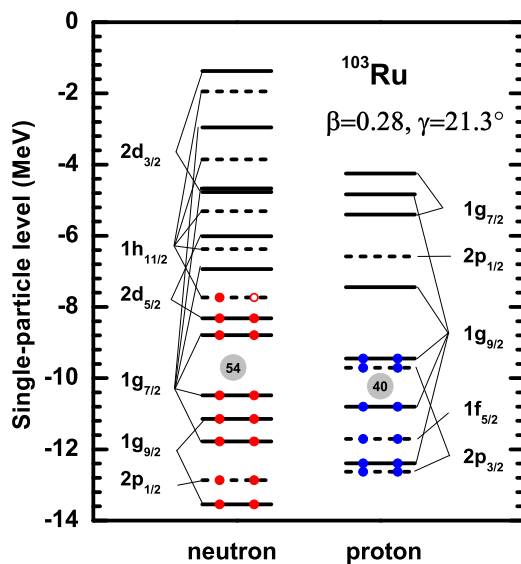


FIG. 2. Single-neutron (left) and single-proton (right) energy levels near the Fermi surface for the ground states in ^{103}Ru . Occupations of nucleons are represented by filled circles.

Therefore, the ground state of ^{103}Ru satisfies both conditions for the wobbling mode.

The ground state deformation parameters of different nuclei can be found accurately and intuitively through the potential energy surface. In addition to the ground state, some excited states might also have wobbling modes. For this purpose, the PECs, i.e., the energy as function of β , for ^{95}Kr , ^{97}Sr , ^{99}Zr , ^{101}Mo , ^{103}Ru , ^{105}Pd , and ^{107}Cd are calculated by the adiabatic constrained CDFT calculations and shown in Fig. 3 (left panels). In the calculations, the constrained calculations with $(\hat{Q}_{20}^2 + 2\hat{Q}_{22}^2)$, i.e., β^2 , are carried out with the triaxial deformation obtained automatically by minimizing the energy. In Fig. 3, the open circles represent the results of adiabatic calculations. They are somewhat irregular energy curves. In addition, some local minima are too vague to distinguish. The configuration fixed calculations can solve this problem well [43]. The corresponding results are shown by lines in Fig. 3. The minimum in each curve is denoted by a red star and labeled by the capital letters A, B, C, ... in accordance with the increasing β value. It can be observed that the ground state deformation parameters in the configuration fixed calculation results, such as local minima B in ^{95}Kr , G in ^{97}Sr , E in ^{99}Zr , G in ^{101}Mo , C in ^{103}Ru , A in ^{105}Pd , and A in ^{107}Cd , are consistent with the two-dimensional β - γ constraint calculations in Fig. 1.

Focusing on ^{95}Kr in the Fig. 3, one can find that there are several excited states with different configuration besides the ground state. For instance, A ($\beta = 0.22$, $\gamma = 35.9^\circ$), C ($\beta = 0.36$, $\gamma = 60^\circ$), D ($\beta = 0.40$, $\gamma = 0^\circ$), E ($\beta = 0.51$, $\gamma = 5.85^\circ$), and F ($\beta = 0.59$, $\gamma = 0^\circ$). Obviously, the state A has remarkable triaxial deformation, which supports it

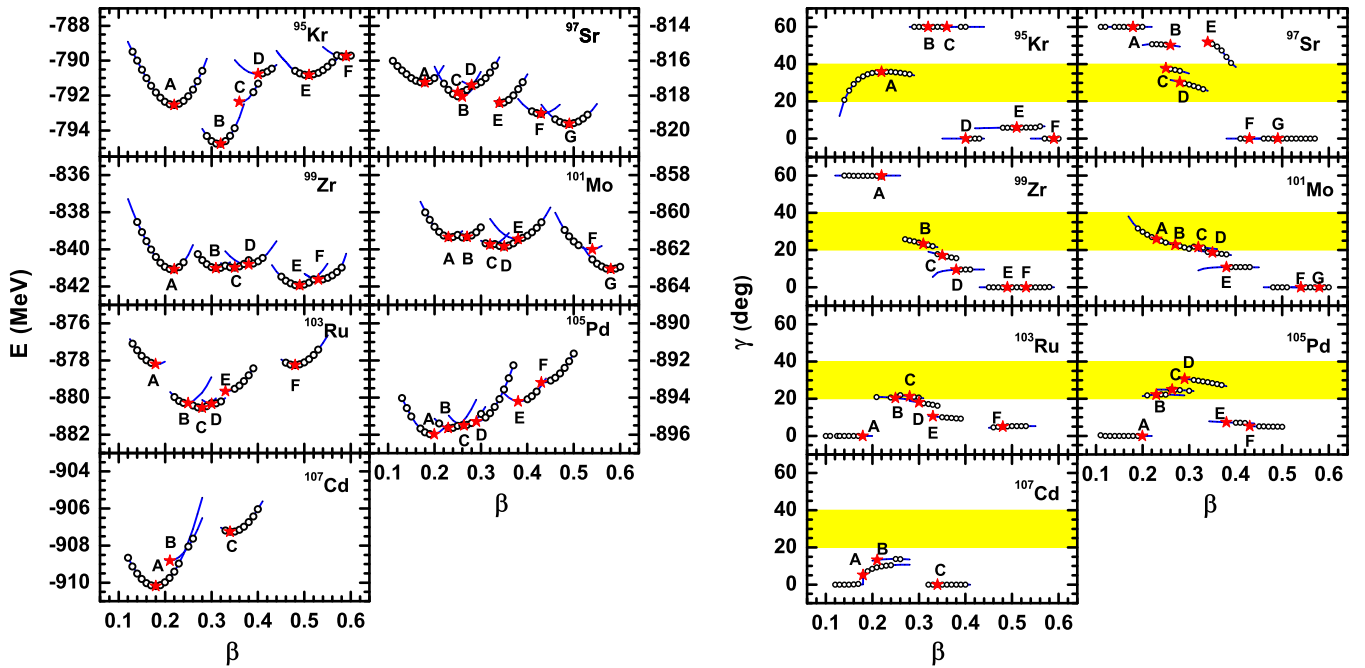


FIG. 3. The potential energy curves (left panels) and the triaxial deformations γ (right panels) as functions of deformation β in adiabatic (open circles) and configuration fixed (solid lines) constrained triaxial CDFT calculation for ^{95}Kr , ^{97}Sr , ^{99}Zr , ^{101}Mo , ^{103}Ru , ^{105}Pd , and ^{107}Cd . The local minima in the energy surfaces for the fixed configuration are represented as stars and labeled as A, B, C, . . . in accordance with the increasing β value. The shaded areas in the right panel of the figure represent the triaxial deformation beneficial to the wobbling mode.

establishing the wobbling motion. It is interesting to note that the excited states of other nuclei also have significant triaxial deformation, which indicates that they might have wobbling modes as well. The states are as follows: A ($\beta = 0.22$, $\gamma = 35.9^\circ$) in ^{95}Kr , C ($\beta = 0.25$, $\gamma = 37.9^\circ$), and D ($\beta = 0.28$, $\gamma = 30.0^\circ$) in ^{97}Sr ; B ($\beta = 0.31$, $\gamma = 23.3^\circ$) in ^{99}Zr ; A ($\beta = 0.23$, $\gamma = 25.9^\circ$), B ($\beta = 0.27$, $\gamma = 22.9^\circ$), and C ($\beta = 0.32$, $\gamma = 21.6^\circ$) in ^{101}Mo ; B ($\beta = 0.25$, $\gamma = 20.4^\circ$) in ^{103}Ru ; as well as B ($\beta = 0.23$, $\gamma = 22.2^\circ$), C ($\beta = 0.27$, $\gamma = 24.9^\circ$), and D ($\beta = 0.29$, $\gamma = 30.7^\circ$) in ^{105}Pd . One notes that the wobbling bands originating from the state C in ^{105}Pd have been reported experimentally [32].

In order to see more intuitively the evolution of nuclear triaxial deformation with respect to β , the deformations γ as functions of deformation β in adiabatic (open circles) and configuration fixed (solid lines) constrained triaxial CDFT calculations for ^{95}Kr , ^{97}Sr , ^{99}Zr , ^{101}Mo , ^{103}Ru , ^{105}Pd , and ^{107}Cd are presented in the right panels of Fig. 3. The shaded area in each figure represents the triaxial deformation beneficial to the wobbling mode. For each configuration, the triaxial deformation varies smoothly with respect to β , which further supports that the deformation γ is mainly determined by its corresponding configuration. In addition, it can be observed that all nuclei except ^{107}Cd show the possible existence of remarkable triaxial deformation.

To show the detailed results of the configuration fixed constrained CDFT calculations, the obtained energies, deformation parameters β and γ , as well as the corresponding valence nucleon and the unpaired nucleon configurations for the local minima in ^{95}Kr , ^{97}Sr , ^{99}Zr , ^{101}Mo , ^{103}Ru , ^{105}Pd , and

^{107}Cd are summarized in Table I. Note that only the information of the orbitals that are not fully occupied in a j shell are listed when writing the valence configuration. From the table, one sees the following states satisfy both significant triaxial deformation and a high- j particle conditions: D ($\beta = 0.28$, $\gamma = 30.0^\circ$) in ^{97}Sr ; B ($\beta = 0.31$, $\gamma = 23.3^\circ$) in ^{99}Zr ; B ($\beta = 0.27$, $\gamma = 22.9^\circ$) and C ($\beta = 0.32$, $\gamma = 21.6^\circ$) in ^{101}Mo ; and C ($\beta = 0.26$, $\gamma = 24.9^\circ$) in ^{105}Pd . Thus the excited states in the ^{97}Sr , ^{99}Zr , ^{101}Mo , and ^{105}Pd nucleus can form wobbling modes. Their unpaired nucleon configurations are all based on $\nu(1h_{11/2})^1$. In particular, there are two configurations suitable for wobbling mode in ^{101}Mo , indicating that it could be a multiple wobbling mode nucleus, which represents an important manifestation of triaxial shape coexistence.

B. Particle rotor model results

It is noteworthy that the configuration with an $h_{11/2}$ neutron was previously identified in the deformed negative parity bands observed in ^{97}Sr and ^{99}Zr [56]. The configuration $\nu h_{11/2}$ was assigned to the $7/2^-$ band in ^{97}Sr and the $11/2^-$ band in ^{99}Zr . The experimental excitation energy of the bandhead state is 0.771 MeV ($I = 7/2\hbar$) in ^{97}Sr and 0.821 MeV ($I = 11/2\hbar$) in ^{99}Zr , which is a bit of a deviation from the theoretical prediction of 2.2 MeV in ^{97}Sr while it is consistent with that of 0.92 MeV in ^{99}Zr (cf. Table I).

To investigate the rotational behavior of the predicted configurations and judge the possible wobbling mode of the nucleus, the PRM [3, 17, 52–54] is adopted. The PRM couples a high- j particle to the triaxial rotor core. The corresponding

TABLE I. The configurations (both valence and unpaired nucleon) as well as the corresponding energies (in MeV) and the deformation parameters β and γ (in degrees) for the local minima in ^{95}Kr , ^{97}Sr , ^{99}Zr , ^{101}Mo , ^{103}Ru , ^{105}Pd , and ^{107}Cd obtained by the configuration fixed constraint triaxial CDFT calculations.

Nucleus	State	Valence	Unpaired	Energy	β	γ
^{95}Kr	A	$\pi(2p_{3/2})^2 \otimes \nu[(1g_{7/2})^4(2d_{3/2})^1]$	$\nu(2d_{3/2})^1$	-792.53	0.22	35.9°
	B	$\pi(1g_{9/2})^2 \otimes \nu(1h_{11/2})^1$	$\nu(1h_{11/2})^1$	-794.75	0.32	60°
	C	$\pi(1g_{9/2})^2 \otimes \nu[(2p_{1/2})^1(1h_{11/2})^2]$	$\nu(2p_{1/2})^1$	-792.35	0.36	60°
	D	$\pi[(2p_{3/2})^2(1f_{5/2})^4] \otimes \nu(1h_{11/2})^3$	$\nu(1h_{11/2})^1$	-790.77	0.40	0°
	E	$\pi[(1g_{9/2})^4(1f_{5/2})^4] \otimes \nu[(1g_{9/2})^{-1}(1h_{11/2})^4]$	$\nu(1h_{11/2})^1$	-790.82	0.51	5.9°
	F	$\pi[(1f_{5/2})^4(2p_{3/2})^2] \otimes \nu[(2d_{5/2})^1(1g_{7/2})^1(1h_{11/2})^2]$	$\nu 2d_{5/2}^1$	-789.75	0.59	0°
^{97}Sr	A	$\pi(2p_{3/2}) \otimes \nu(2d_{5/2})^3$	$\nu(2d_{5/2})^1$	-817.24	0.18	60°
	B	$\pi[(2p_{3/2})^2(1g_{9/2})^2] \otimes \nu(1g_{7/2})^3$	$\nu(1g_{7/2})^1$	-818.05	0.26	50.2°
	C	$\pi[(1g_{9/2})^2(2p_{3/2})^2] \otimes \nu[(2d_{3/2})^{-1}(1g_{7/2})^{-2}]$	$\nu(2d_{3/2})^1$	-817.80	0.25	37.9°
	D	$\pi[(2p_{3/2})^2(1g_{9/2})^2] \otimes \nu[(1h_{11/2})^1(1g_{7/2})^{-2}(2d_{5/2})^2]$	$\nu(1h_{11/2})^1$	-817.40	0.28	30.4°
	E	$\pi(1g_{9/2})^4 \otimes \nu[(2d_{3/2})^{-1}(2d_{5/2})^2(1g_{7/2})^2]$	$\nu(2d_{3/2})^1$	-818.41	0.34	51.9°
	F	$\pi[(1g_{9/2})^4(2p_{3/2})^2] \otimes \nu(1h_{11/2})^3$	$\nu(1h_{11/2})^1$	-812.13	0.43	0°
	G	$\pi[(2p_{3/2})^2(1g_{9/2})^4] \otimes \nu(1g_{9/2})^{-1}$	$\nu(1g_{9/2})^1$	-819.62	0.49	0°
^{99}Zr	A	$\pi[(2p_{3/2})(1g_{9/2}^2(1f_{5/2})^{-2})] \otimes \nu(1g_{7/2})^{-1}$	$\nu(1g_{7/2})^1$	-841.07	0.22	60°
	B	$\pi(1g_{9/2})^4 \otimes \nu(1h_{11/2})^1$	$\nu(1h_{11/2})^1$	-841.02	0.31	23.3°
	C	$\pi[(1f_{5/2})(1g_{9/2})^4] \otimes \nu[(2d_{5/2})^3(1g_{7/2})^4]$	$\nu(2d_{5/2})^1$	-840.98	0.35	17.1°
	D	$\pi[(1f_{5/2})(2p_{3/2})^2(1g_{9/2})^4] \otimes \nu[(1h_{11/2})^3(1g_{7/2})^4]$	$\nu(1h_{11/2})^1$	-840.82	0.38	9.4°
	E	$\pi[(1g_{9/2})^6(2p_{3/2})^2(1f_{5/2})^4] \otimes \nu[(1g_{9/2})^{-1}(1h_{11/2})^4(1g_{7/2})^4]$	$\nu(1g_{9/2})^1$	-841.94	0.49	0°
	F	$\pi[(1g_{9/2})^6(2p_{3/2})^2] \otimes \nu[(1h_{11/2})^5(1g_{7/2})^2]$	$\nu((1h_{11/2})^1)$	-841.63	0.53	0°
	G	$\pi(1g_{9/2})^4 \otimes \nu[(1g_{7/2})^{-3}(2d_{5/2})^{-2}]$	$\nu(1g_{7/2})^1$	-861.34	0.23	25.9°
^{101}Mo	A	$\pi[(2p_{3/2})(1g_{9/2})^4] \otimes \nu[(1h_{11/2})^1(1g_{7/2})^6]$	$\nu(1h_{11/2})^1$	-861.34	0.27	22.9°
	B	$\pi(1g_{9/2})^6 \otimes \nu[(1h_{11/2})^1(1g_{7/2})^6]$	$\nu(1h_{11/2})^1$	-861.74	0.32	21.6°
	C	$\pi(1g_{9/2})^6 \otimes \nu[(2d_{5/2})^1(1g_{7/2})^6]$	$\nu(2d_{5/2})^1$	-861.85	0.35	18.7°
	D	$\pi(1g_{9/2})^6 \otimes \nu[(1h_{11/2})^3(1g_{7/2})^6]$	$\nu(1h_{11/2})^1$	-861.44	0.38	10.9°
	E	$\pi[(1g_{7/2})^2(1g_{9/2})^6] \otimes \nu[(1g_{9/2})^{-1}(1g_{7/2})^4(1h_{11/2})^4]$	$\nu(1g_{9/2})^1$	-862.00	0.54	0°
	F	$\pi[(2d_{3/2})^2(1g_{9/2})^6] \otimes \nu[(1h_{11/2})^5(1g_{7/2})^4(1g_{9/2})^{-2}]$	$\nu(1h_{11/2})^1$	-863.06	0.58	0°
	G	$\pi(1g_{9/2})^4 \otimes \nu[(1g_{7/2})^{-3}(2d_{5/2})^2]$	$\nu(1g_{7/2})^1$	-878.20	0.18	0°
^{103}Ru	A	$\pi(1g_{9/2})^6 \otimes \nu[(1g_{7/2})^{-3}(2d_{5/2})^2]$	$\nu(1g_{7/2})^1$	-880.30	0.25	20.4°
	B	$\pi(1g_{9/2})^6 \otimes \nu[(1h_{11/2})^1(2d_{5/2})^2]$	$\nu(1h_{11/2})^1$	-880.55	0.28	21.3°
	C	$\pi[(1g_{9/2})^6(2p_{3/2})] \otimes \nu[(2d_{5/2})^1(1g_{7/2})^{-2}(1h_{11/2})^2]$	$\nu(2d_{5/2})^1$	-880.34	0.30	18.01°
	D	$\pi[(2p_{3/2})(1g_{9/2})^6] \otimes \nu[(1h_{11/2})^3(1g_{7/2})^4(2d_{5/2})^2]$	$\nu(1h_{11/2})^1$	-879.66	0.33	10.5°
	E	$\pi(1f_{5/2}) \otimes \nu[(1g_{9/2})^{-1}(1h_{11/2})^4]$	$\nu(1g_{9/2})^1$	-878.24	0.48	5.0°
	F	$\pi(1g_{9/2})^6 \otimes \nu[(1g_{7/2})^5(2d_{5/2})^4]$	$\nu(1g_{7/2})^1$	-895.97	0.19	0°
	G	$\pi(1g_{9/2})^{-2} \otimes \nu[(1g_{7/2})^5(2d_{5/2})^4]$	$\nu(1g_{7/2})^1$	-895.65	0.23	22.2°
^{105}Pd	A	$\pi(1g_{9/2})^{-2} \otimes \nu[(1h_{11/2})^1(1g_{7/2})^6(2d_{3/2})^2]$	$\nu(1h_{11/2})^1$	-895.49	0.27	24.9°
	B	$\pi(1g_{9/2})^{-2} \otimes \nu[(1g_{7/2})^5(2d_{3/2})^2(1h_{11/2})^2]$	$\nu(1g_{7/2})^1$	-895.29	0.29	30.7°
	C	$\pi[(1g_{7/2})^2(1g_{9/2})^6] \otimes \nu[(1h_{11/2})^3(1g_{7/2})^6]$	$\nu(1h_{11/2})^1$	-894.21	0.38	7.3°
	D	$\pi(2p_{3/2})^2 \otimes \nu[(1g_{9/2})^{-1}(1h_{11/2})^4]$	$\nu(1g_{9/2})^1$	-893.18	0.43	5.2°
	E	$\pi(1g_{9/2})^{-2} \otimes \nu[(1g_{7/2})^5(2d_{5/2})^{-2}]$	$\nu(1g_{7/2})^1$	-910.18	0.18	5.1°
	F	$\pi(1g_{9/2})^{-2} \otimes \nu[(1h_{11/2})^1(2d_{5/2})^4(1g_{7/2})^4]$	$\nu(1h_{11/2})^1$	-908.81	0.21	13.2°
^{107}Cd	A	$\pi[(1g_{7/2})^2(1g_{9/2})^6] \otimes \nu[(1h_{11/2})^3(2d_{5/2})^2(1g_{7/2})^4]$	$\nu(1h_{11/2})^1$	-907.25	0.34	0°

Hamiltonian is

$$H_{\text{PRM}} = \sum_{k=1,2,3} \frac{(\hat{J}_k - \hat{j}_k)^2}{2\mathcal{J}_k(\beta, \gamma)} + h_p(\gamma), \quad (5)$$

$$h_p(\gamma) = \frac{C}{2} \left\{ \cos \gamma \left[\hat{j}_3^2 - \frac{j(j+1)}{3} \right] + \frac{\sin \gamma}{2\sqrt{3}} (\hat{j}_+^2 + \hat{j}_-^2) \right\}, \quad (6)$$

where \hat{J}_k is the total angular momentum, \hat{j}_k the angular momentum of the particle, and C the single- j shell Hamiltonian coupling strength to the deformed potential.

In PRM calculations, the input deformation parameters (β, γ) are $(0.28, 30.4^\circ)$ for ^{97}Sr and $(0.31, 23.3^\circ)$ for ^{99}Zr , which are obtained from the CDFT calculations (cf. Table I). The single- j shell Hamiltonian parameter C is taken as

$$C = \left(\frac{123}{8} \sqrt{\frac{5}{\pi}} \right) \frac{2N+3}{j(j+1)} A^{-1/3} \beta. \quad (7)$$

The irrotational flow type of moment of inertia $\mathcal{J}_k(\gamma) = \mathcal{J}_0 \sin^2(\gamma - 2k\pi/3)$ with $\mathcal{J}_0 = 30 \hbar^2/\text{MeV}$ is used. For the electromagnetic transitions, the empirical intrinsic quadrupole moment of $Q = (3/\sqrt{5\pi}) R_0^2 Z\beta$ and the gyromagnetic ratios of $g_R = Z/(A-1)$ and $g_v(h_{11/2}) = -0.21$ are adopted.

The obtained energy spectra (labeled as bands B1 and B1'), $B(E2)_{\text{out}}/B(E2)_{\text{in}}$, as well as $B(M1)_{\text{out}}/B(E2)_{\text{in}}$ values of ^{97}Sr and ^{99}Zr are displayed in Fig. 4 in comparison with the available experimental energy spectra. The experimental results are reproduced well. In addition, the HFA method [2] is also used to study the wobbling mode in this paper, and the calculations are expressed by blue solid lines in Fig. 4.

The energy difference is an essential criterion for judging the type of wobbling motion. The energy difference between bands B1 and B1' is defined as

$$\Delta E(I) = E_{B1'}(I) - \frac{1}{2}[E_{B1}(I+1) + E_{B1}(I-1)]. \quad (8)$$

In both PRM and HFA calculations, the energy difference in the low spin region decreases with the increase of spin, which is usually regarded as a prominent feature of the transverse wobbling mode [2,3]. Compared with the calculation of PRM, the result of HFA decreases more rapidly [cf. Figs. 4(c) and 4(d)]. This can be attributed to the small-amplitude assumption in the HFA underestimating the critical angular momentum at which the TW collapses [3]. We must also consider that the wobbling motion discussed in the PRM disrupts the small amplitude depiction in the HFA, making it nonharmonic. For the higher spin region, the wobbling energy in PRM will go up, similar to that in ^{135}Pr (cf. Fig. 16 of Ref. [2]). We further note that the calculated wobbling energy in the PRM is in general a bit smaller in comparison to those in ^{135}Pr (cf. Fig. 16 of Ref. [2]). This can be interpreted that the wobbling energy is closely related to the moment of inertia; in particular it is inversely proportional to the s -axis moment of inertia (cf. Eq. (24) of Ref. [2]). The s -axis moment of inertia in ^{135}Pr ($\mathcal{J}_s = 6 \hbar^2/\text{MeV}$) (cf. Table I of Ref. [2]) is smaller than that of ^{97}Sr ($\mathcal{J}_s = 7.9 \hbar^2/\text{MeV}$) and ^{99}Zr ($\mathcal{J}_s = 10.7 \hbar^2/\text{MeV}$). Hence, the wobbling energies in ^{97}Sr and ^{99}Zr are a bit smaller than that in ^{135}Pr .

The calculated electromagnetic transition probability ratios $B(E2)_{\text{out}}/B(E2)_{\text{in}}$ and $B(M1)_{\text{out}}/B(E2)_{\text{in}}$ from the PRM and

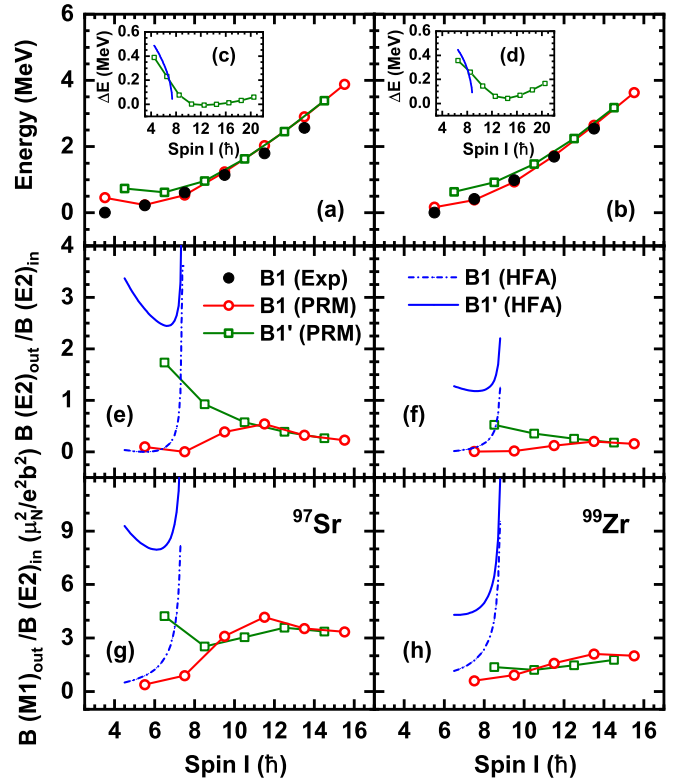


FIG. 4. The lowest bands B1 and B1' based on the configuration $\nu h_{11/2}^1$ in ^{97}Sr and ^{99}Zr . (a)–(b) The calculated energy spectra by PRM are compared with the experimental data in Ref. [56]. (c)–(d) Theoretical energy difference between the doublet bands B1 and B1'. (e)–(h) The $B(E2)_{\text{out}}/B(E2)_{\text{in}}$ and $B(M1)_{\text{out}}/B(E2)_{\text{in}}$ values for the interband transitions from band B1' to B1 calculated by the PRM and HFA.

HFA for B1' and B1 bands are shown in Figs. 4(e)–4(h). The results of HFA are larger than those of PRM. This is because with the assumption of a frozen alignment along the s axis the HFA does not take into account the collective rotational effects induced by the intermediate (m) axis, so that it underestimates $B(E2)_{\text{in}}$. The ratio $B(E2)_{\text{out}}/B(E2)_{\text{in}}$ of PRM is large (≥ 0.5) in the whole spin region, indicating that the $E2$ transitions from band B1 to band B1' are highly collective. This is the fingerprint of TW, which represents a wobbling of the triaxial charge density with respect to the angular momentum vector. The ratio decreases with increasing angular momentum I . Unlike PRM, the HFA results decrease first and increase rapidly at large I , when the TW collapses.

The change of $B(M1)_{\text{out}}/B(E2)_{\text{in}}$ value with I is not monotonic in ^{97}Sr and ^{99}Zr . They show a decrease first and then an increase. In the PRM, the turning point is $I = 17/2\hbar$ for ^{97}Sr and $I = 21/2\hbar$ for ^{99}Zr . In the HFA, the turning point is earlier, consistent with the earlier disappearance of TW mode. This implies that the behavior of the $B(M1)_{\text{out}}/B(E2)_{\text{in}}$ can be used to identify the collapses of the TW. One notes that the $B(M1)_{\text{out}}/B(E2)_{\text{in}}$ values are not small, as expected for a wobbling motion. One understands that the wobbling motion is coupled to the vibrations of the proton and neutron currents against each other, i.e., the scissor mode, which can

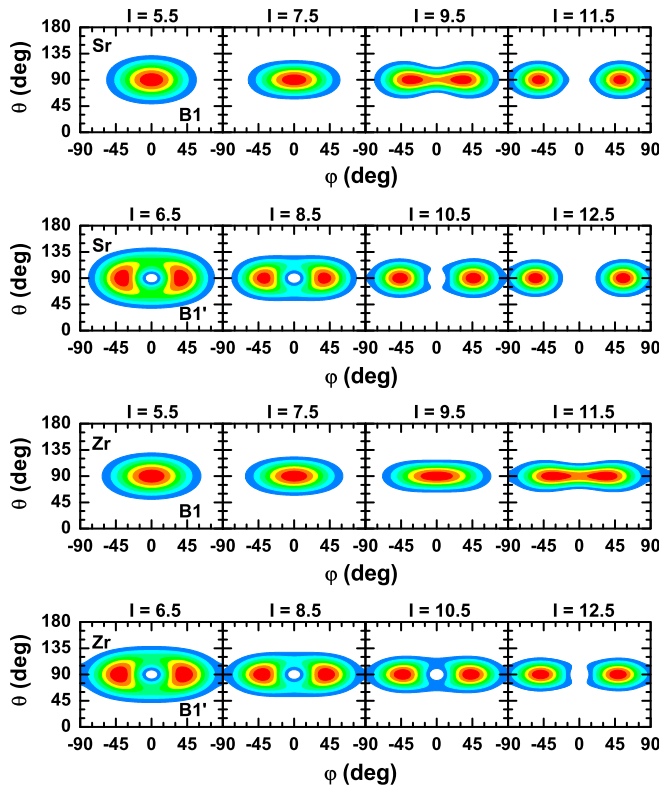


FIG. 5. The SCS maps, i.e., probability density profiles for the orientation of the angular momentum I on the (θ, φ) plane, calculated by PRM for the doublet bands B1 and B1' in ^{97}Sr and ^{99}Zr . Here, θ is the angle between the total angular momentum \mathbf{J} and the l axis, and φ is the angle between the projection of \mathbf{J} onto the sm plane and the s axis. The color sequence with increasing probability is white, blue, green, yellow, red.

draw the $M1$ strength [57] but is not taken into in the PRM calculations. In Fig. 4, the results of $B(M1)_{\text{out}}/B(E2)_{\text{in}}$ and $B(E2)_{\text{out}}/B(E2)_{\text{in}}$ for the transitions from the band B1 to B1' are further presented. A staggering difference between the transitions of B1' \rightarrow B1 and B1 \rightarrow B1' is observed and further supports that they are wobbling partner bands [58].

We have further checked that the calculated mixing ratios $\delta = \langle E2 \rangle_{\text{out}} / \langle M1 \rangle_{\text{out}}$ are positive. This is a hallmark of a TW built on a neutron configuration [32], in contrast to that built on a proton configuration with a negative δ value [13,14]. The reason is that the signs of the $g_n - g_R$ and $g_p - g_R$ factors appearing in the $M1$ operator are opposite [32]. Nevertheless, further experimental efforts are needed to extend the energy level scheme for the partner band and extract the corresponding electromagnetic transition probability data to distinguish between the possible wobbling motion and the other alternative explanations.

To further reveal the nature of the rotational modes for the doublet bands B1 and B1' in ^{97}Sr and ^{99}Zr , the probability density profiles $\mathcal{P}(\theta, \varphi)$ for the orientation of the angular momentum \mathbf{J} on the (θ, φ) plane (called SCS maps [3] or azimuthal plots [52,59]) calculated by the PRM are shown in Fig. 5. As indicated in figure, the probability distributions $\mathcal{P}(\theta, \varphi)$ exhibit a central tendency with respect to the $\theta = 90^\circ$

plane, corresponding to the small long (l) axis component of \mathbf{J} , due to the smallest moment of inertia for the l axis. In ^{97}Sr , band B1 exhibits the characteristics of a zero-phonon state in its angular momentum orientation profile. The distribution is characterized by the property of symmetry with respect to $\varphi = 0^\circ$ and attains its maximum value at $\varphi = 0^\circ$ when $I = 11/2\hbar$ and $15/2\hbar$. This maximum corresponds to the optimal alignment of \mathbf{J} with the s axis. As the spin increases, the orientation of \mathbf{J} gradually deviates from the s axis. Driven by the increasing m -axis component from the collective rotor angular momentum, a plane rotation is finally formed in the sm plane at $I = 19/2\hbar$ and approaches the m axis at $I = 23/2\hbar$. For the B1' band, the profile shows that it is a one-phonon wobbling excitation, that is, φ is antisymmetric and the probability minimizes at $\varphi = 0^\circ$. The maximum probability is located around the s axis, reflecting the wobbling motion (precession) of \mathbf{J} around the s axis. For higher spins ($I \geq 21/2\hbar$), the rotation mode eventually becomes sm plane rotation. Therefore, the $\mathcal{P}(\theta, \varphi)$ results support that the TW will occur in the region of $I \leq 17/2\hbar$. Combined with Fig. 4(g), one notes that when the TW collapses the $B(M1)_{\text{out}}/B(E2)_{\text{in}}$ value increases with the spin. Similar behavior can be found for ^{99}Zr from Fig. 5. The results show that the TW can occur in the region of $I \leq 21/2\hbar$. Namely, the TW occurs in a broader spin region than the case of ^{97}Sr , due to a larger $\mathcal{J}_s/\mathcal{J}_m$ ratio when the triaxial deformation γ becomes smaller.

In the present PRM study, we have also obtained valuable insights into the properties of the single-particle-like signature-partner band through our analysis of the energy spectra and electromagnetic transition probabilities, as depicted in Fig. 6. The B2' state is identified as the signature partner and it is evident from the figure that its energy is considerably higher than that of the wobbling band B1', as shown in Fig. 4. Moreover, the ratio $B(E2)_{\text{out}}/B(E2)_{\text{in}}$ in band B2' is found to be very small, suggesting that the excitation from the B1 to B2' state is not a collective phenomenon. We have also evaluated the $B(M1)_{\text{out}}/B(E2)_{\text{in}}$ ratios for the transitions between the B2' and B1 states. We find that the transition probabilities from B2' to B1 are negligible across the spin range. On the other hand, the probability of the B1 \rightarrow B2' transition is significant at low spins, but decreases as spin is increased. This information illuminates the nature of the single-particle-like signature-partner band. Our results demonstrate that these states exhibit features that are distinct from those observed in the wobbling band.

In Fig. 7, we present the probability density profiles $\mathcal{P}(\theta, \varphi)$ for the orientation of the angular momentum \mathbf{J} on the (θ, φ) plane for the band B2' in ^{97}Sr and ^{99}Zr . At spin $I = 13/2\hbar$, the probability of the total angular momentum \mathbf{J} is greatest along the s axis, which is perpendicular to the triaxial symmetry axis. In contrast to the wobbling band B1' (shown in Fig. 5), there is no node in the probability density profile at $\varphi = 0^\circ$, indicating the absence of a collective excitation mode. We have also verified that the particle angular momentum \mathbf{j} undergoes precession around the s axis, as expected for an unfavored signature partner. This precession can be interpreted as a rotation about the s axis with one less unit of particle angular momentum along this axis. As the spin increases, the angular momentum gradually transfers to the sm

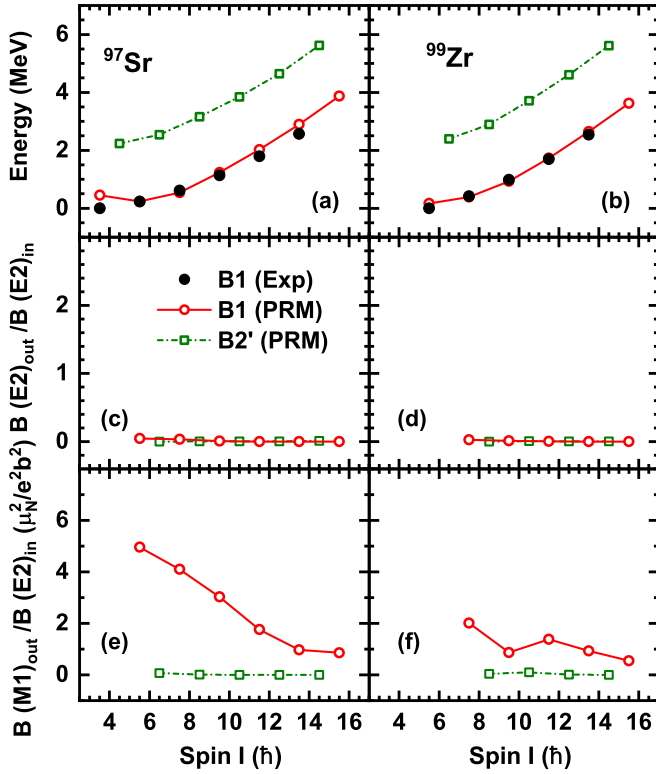


FIG. 6. Same as Fig. 4, but for the lowest band B1 and the single-particle-like signature-partner band B2'.

plane, driven by an increase in the rotor angular momentum along the m axis. Therefore, the angular momentum geometries in the single-particle-like signature-partner band exhibit features distinct from those observed in the wobbling band. Our findings shed light on the complex interplay between single-particle motion, collective excitations, and rotational motion in the wobbling and signature bands.

III. SUMMARY

In summary, adiabatic and configuration fixed constrained triaxial CDFT calculations are used to explore the possible existence of wobbling modes among $N = 59$ isotones ^{95}Kr , ^{97}Sr , ^{99}Zr , ^{101}Mo , ^{103}Ru , ^{105}Pd , and ^{107}Cd in the mass region $A \approx 100$. The corresponding PESs, PECs, deformation parameters, and the configurations for the ground and excited states are obtained. From the adiabatic constraint calculation, the results show that the ground state of ^{103}Ru has a significant triaxial deformation, and the configuration has a high- j particle, which makes it a candidate for a nucleus with wobbling motion. For the excited states, there are several states that satisfy the conditions of high- j valence particles and suitable triaxial deformation in ^{97}Sr , ^{99}Zr , ^{101}Mo , and ^{105}Pd . Interestingly, ^{101}Mo might be a candidate for the triaxial shape coexistence with the possible evidence of multiple wobbling modes.

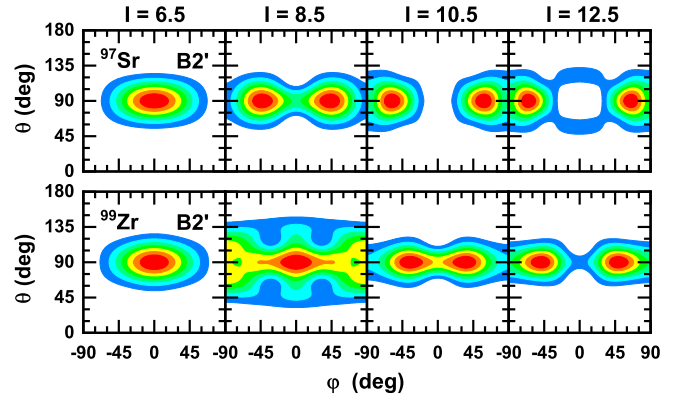


FIG. 7. Same as Fig. 5, but for the single-particle-like signature-partner band B2'.

Furthermore, the rotational bands based on the $\nu(1h_{11/2})^1$ configuration in ^{97}Sr and ^{99}Zr are used as examples to study the nature of the wobbling motion by adopting the PRM and HFA methods. The PRM reproduces the experimental energy spectra well. The results of the energy difference between the doublet bands, the enhanced $B(E2)_{\text{out}}/B(E2)_{\text{in}}$ values, as well as the one-phonon oscillation characteristic of the total angular momentum point to the two nuclei being TW candidates, which suggests the possibility of a larger region of wobbling modes near the $A \approx 100$ mass region. We have also obtained valuable insights into the properties of the single-particle-like signature-partner band through our analysis of the energy spectra, electromagnetic transition probabilities, and the probability density profiles $\mathcal{P}(\theta, \varphi)$ for the orientation of the angular momentum \mathbf{J} on the (θ, φ) plane. Our results demonstrate that these states exhibit features that are distinct from those observed in the wobbling band. Further experimental efforts on extending the level scheme and extracting electromagnetic transition data are certainly necessary to examine the present theoretical predictions.

Finally, we have to bear in mind that our current calculations utilize a single set of deformation parameters obtained from CDFT as input in the PRM. While this approximation is reasonable when the nuclear shape is fixed, it overlooks the correlations between different deformations. However, it is important to note that the shape of the nucleus can be sensitive to various configurations, and these configurations are energetically very close to each other. Thus, for transitional nuclei where shape fluctuations and angular fluctuations are coupled together, our present theoretical framework may not yield accurate results. To address this limitation, future efforts should be directed towards considering the effects of mixing different configurations.

ACKNOWLEDGMENTS

We thank Prof. S. Frauendorf for helpful suggestions. This work was supported by the National Natural Science Foundation of China under Grants No. 12205103 and No. 12175071.

- [1] *Nuclear Structure*, edited by A. Bohr and B. R. Mottelson (Benjamin, New York, 1975), Vol. II.
- [2] S. Frauendorf and F. Dönau, *Phys. Rev. C* **89**, 014322 (2014).
- [3] Q. B. Chen and S. Frauendorf, *Eur. Phys. J. A* **58**, 75 (2022).
- [4] J. H. Hamilton, S. J. Zhu, Y. X. Luo, A. V. Ramayya, S. Frauendorf, J. O. Rasmussen, J. K. Hwang, S. H. Liu, G. M. Ter-Akopian, A. V. Daniel *et al.*, *Nucl. Phys. A* **834**, 28c (2010).
- [5] Y. X. Luo, J. H. Hamilton, A. V. Ramayya, J. K. Hwang, S. H. Liu, J. O. Rasmussen, S. Frauendorf, G. M. Ter-Akopian, A. V. Daniel, and Y. T. Oganessian, *Exotic Nuclei: Exon-2012: Proceedings of the International Symposium* (World Scientific, Singapore, 2013).
- [6] S. W. Ødegård, G. B. Hagemann, D. R. Jensen, M. Bergström, B. Herskind, G. Sletten, S. Törmänen, J. N. Wilson, P. O. Tjøm, I. Hamamoto, K. Spohr, H. Hubel, A. Gorgen, G. Schonwasser, A. Bracco, S. Leoni, A. Maj, C. M. Petrache, P. Bednarczyk, and D. Curien, *Phys. Rev. Lett.* **86**, 5866 (2001).
- [7] D. R. Jensen, G. B. Hagemann, I. Hamamoto, S. W. Ødegård, B. Herskind, G. Sletten, J. N. Wilson, K. Spohr, H. Hübel, P. Bringel, A. Neusser, G. Schonwasser, A. K. Singh, W. C. Ma, H. Amro, A. Bracco, S. Leoni, G. Benzoni, A. Maj *et al.*, *Phys. Rev. Lett.* **89**, 142503 (2002).
- [8] P. Bringel, G. B. Hagemann, H. Hübel, A. Al-Khatib, P. Bednarczyk, A. Bürger, D. Curien, G. Gangopadhyay, B. Herskind, D. R. Jensen *et al.*, *Eur. Phys. J. A* **24**, 167 (2005).
- [9] G. Schönwaßer, H. Hübel, G. B. Hagemann, P. Bednarczyk, G. Benzoni, A. Bracco, P. Bringel, R. Chapman, D. Curien, J. Domscheit *et al.*, *Phys. Lett. B* **552**, 9 (2003).
- [10] H. Amro, W. C. Ma, G. B. Hagemann, R. M. Diamond, J. Domscheit, P. Fallon, A. Gørgen, B. Herskind, H. Hübel, D. R. Jensen *et al.*, *Phys. Lett. B* **553**, 197 (2003).
- [11] D. J. Hartley, R. V. F. Janssens, L. L. Riedinger, M. A. Riley, A. Aguilar, M. P. Carpenter, C. J. Chiara, P. Chowdhury, I. G. Darby, U. Garg, Q. A. Ijaz, F. G. Kondev, S. Lakshmi, T. Lauritsen, A. Ludington, W. C. Ma, E. A. McCutchan, S. Mukhopadhyay, R. Pifer, E. P. Seyfried *et al.*, *Phys. Rev. C* **80**, 041304(R) (2009).
- [12] A. Mukherjee, S. Bhattacharya, T. Trivedi, S. Tiwari, R. P. Singh, S. Muralithar, K. Katre, R. Kumar, R. Palit, S. Chakraborty, Yashraj, S. Jehangir, N. Nazir, S. P. Rouoof, G. H. Bhat, J. A. Sheikh, N. Rather, R. Raut, S. S. Ghugre, S. Ali *et al.*, *Phys. Rev. C* **107**, 054310 (2023).
- [13] J. T. Matta, U. Garg, W. Li, S. Frauendorf, A. D. Ayangeakaa, D. Patel, K. W. Schllax, R. Palit, S. Saha, J. Sethi *et al.*, *Phys. Rev. Lett.* **114**, 082501 (2015).
- [14] N. Sensharma, U. Garg, S. Zhu, A. D. Ayangeakaa, S. Frauendorf, W. Li, G. Bhat, J. A. Sheikh, M. P. Carpenter, Q. B. Chen *et al.*, *Phys. Lett. B* **792**, 170 (2019).
- [15] S. Biswas, R. Palit, S. Frauendorf, U. Garg, W. Li, G. H. Bhat, J. A. Sheikh, J. Sethi, S. Saha, P. Singh *et al.*, *Eur. Phys. J. A* **55**, 159 (2019).
- [16] C. M. Petrache, P. M. Walker, S. Guo, Q. B. Chen, S. Frauendorf, Y. X. Liu, R. A. Wyss, D. Mengoni, Y. H. Qiang, A. Astier *et al.*, *Phys. Lett. B* **795**, 241 (2019).
- [17] Q. B. Chen, S. Frauendorf, and C. M. Petrache, *Phys. Rev. C* **100**, 061301(R) (2019).
- [18] Y. K. Wang, F. Q. Chen, and P. W. Zhao, *Phys. Lett. B* **802**, 135246 (2020).
- [19] S. Chakraborty, H. P. Sharma, S. S. Tiwary, C. Majumder, A. K. Gupta, P. Banerjee, S. Ganguly, S. Rai, S. Kumar, A. Kumar *et al.*, *Phys. Lett. B* **811**, 135854 (2020).
- [20] K. R. Devi, S. Kumar, N. Kumar, F. S. Babra, M. S. Laskar, S. Biswas, S. Saha, P. Singh, S. Samanta, S. Das *et al.*, *Phys. Lett. B* **823**, 136756 (2021).
- [21] B. F. Lv, C. M. Petrache, R. Budaca, A. Astier, K. K. Zheng, P. Greenlees, H. Badran, T. Calverley, D. M. Cox, T. Grahn *et al.*, *Phys. Rev. C* **105**, 034302 (2022).
- [22] N. Sensharma, U. Garg, Q. B. Chen, S. Frauendorf, D. P. Burdette, J. L. Cozzi, K. B. Howard, S. Zhu, M. P. Carpenter, P. Copp *et al.*, *Phys. Rev. Lett.* **124**, 052501 (2020).
- [23] S. Nandi, G. Mukherjee, Q. B. Chen, S. Frauendorf, R. Banik, S. Bhattacharya, S. Dar, S. Bhattacharyya, C. Bhattacharya, S. Chatterjee *et al.*, *Phys. Rev. Lett.* **125**, 132501 (2020).
- [24] S. Frauendorf, *Phys. Rev. C* **97**, 069801 (2018).
- [25] K. Tanabe and K. Sugawara-Tanabe, *Phys. Rev. C* **97**, 069802 (2018).
- [26] E. A. Lawrie, O. Shirinda, and C. M. Petrache, *Phys. Rev. C* **101**, 034306 (2020).
- [27] B. F. Lv, C. M. Petrache, E. A. Lawrie, A. Astier, E. Dupont, K. K. Zheng, P. Greenlees, H. Badran, T. Calverley, D. M. Cox, T. Grahn, J. Hilton, R. Julin, S. Juutinen, J. Konki, J. Pakarinen, P. Papadakis, J. Partanen, P. Rahkila *et al.*, *Phys. Rev. C* **103**, 044308 (2021).
- [28] K. Tanabe and K. Sugawara-Tanabe, *Phys. Rev. C* **95**, 064315 (2017).
- [29] B. F. Lv, C. M. Petrache, E. A. Lawrie, S. Guo, A. Astier, K. K. Zheng, H. J. Ong, J. G. Wang, X. H. Zhou, Z. Y. Sun *et al.*, *Phys. Lett. B* **824**, 136840 (2022).
- [30] S. Guo, X. H. Zhou, C. M. Petrache, E. A. Lawrie, S. H. Mthembu, Y. D. Fang, H. Y. Wu, H. L. Wang, H. Y. Meng, G. S. Li *et al.*, *Phys. Lett. B* **828**, 137010 (2022).
- [31] K. Nomura and C. M. Petrache, *Phys. Rev. C* **105**, 024320 (2022).
- [32] J. Timár, Q. B. Chen, B. Kruzsicz, D. Sohler, I. Kuti, S. Q. Zhang, J. Meng, P. Joshi, R. Wadsworth, K. Starosta *et al.*, *Phys. Rev. Lett.* **122**, 062501 (2019).
- [33] C. Vaman, D. B. Fossan, T. Koike, K. Starosta, I. Y. Lee, and A. O. Macchiavelli, *Phys. Rev. Lett.* **92**, 032501 (2004).
- [34] E. O. Lieder, R. M. Lieder, R. A. Bark, Q. B. Chen, S. Q. Zhang, J. Meng, E. A. Lawrie, J. J. Lawrie, S. P. Bvumbi, N. Y. Kheswa *et al.*, *Phys. Rev. Lett.* **112**, 202502 (2014).
- [35] N. Rather, P. Datta, S. Chattopadhyay, S. Rajbanshi, A. Goswami, G. H. Bhat, J. A. Sheikh, S. Roy, R. Palit, S. Pal *et al.*, *Phys. Rev. Lett.* **112**, 202503 (2014).
- [36] D. Tonev, M. S. Yavahchova, N. Goutev, G. de Angelis, P. Petkov, R. K. Bhowmik, R. P. Singh, S. Muralithar, N. Madhavan, R. Kumar *et al.*, *Phys. Rev. Lett.* **112**, 052501 (2014).
- [37] I. Kuti, Q. B. Chen, J. Timár, D. Sohler, S. Q. Zhang, Z. H. Zhang, P. W. Zhao, J. Meng, K. Starosta, T. Koike *et al.*, *Phys. Rev. Lett.* **113**, 032501 (2014).
- [38] P.-G. Reinhard, *Rep. Prog. Phys.* **52**, 439 (1989).
- [39] P. Ring, *Prog. Part. Nucl. Phys.* **37**, 193 (1996).
- [40] D. Vretenar, A. V. Afanasjev, G. A. Lalazissis, and P. Ring, *Phys. Rep.* **409**, 101 (2005).
- [41] J. Meng, H. Toki, S.-G. Zhou, S. Q. Zhang, W. H. Long, and L. S. Geng, *Prog. Part. Nucl. Phys.* **57**, 470 (2006).
- [42] *Relativistic Density Functional for Nuclear Structure*, International Review of Nuclear Physics Vol. 10, edited by J. Meng (World Scientific, Singapore, 2016).
- [43] J. Meng, J. Peng, S. Q. Zhang, and S.-G. Zhou, *Phys. Rev. C* **73**, 037303 (2006).

- [44] J. Peng, H. Sagawa, S. Q. Zhang, J. M. Yao, Y. Zhang, and J. Meng, *Phys. Rev. C* **77**, 024309 (2008).
- [45] J. M. Yao, B. Qi, S. Q. Zhang, J. Peng, S. Y. Wang, and J. Meng, *Phys. Rev. C* **79**, 067302 (2009).
- [46] J. Li, S. Q. Zhang, and J. Meng, *Phys. Rev. C* **83**, 037301 (2011).
- [47] J. Peng and Q. B. Chen, *Phys. Rev. C* **98**, 024320 (2018).
- [48] B. Qi, H. Jia, C. Liu, and S. Y. Wang, *Phys. Rev. C* **98**, 014305 (2018).
- [49] J. Li, *Phys. Rev. C* **97**, 034306 (2018).
- [50] S. Frauendorf and J. Meng, *Nucl. Phys. A* **617**, 131 (1997).
- [51] L. Hu, J. Peng, and Q. B. Chen, *Phys. Rev. C* **104**, 064325 (2021).
- [52] E. Streck, Q. B. Chen, N. Kaiser, and U.-G. Meißner, *Phys. Rev. C* **98**, 044314 (2018).
- [53] Q. B. Chen, S. Frauendorf, N. Kaiser, U.-G. Meißner, and J. Meng, *Phys. Lett. B* **807**, 135596 (2020).
- [54] C. Broocks, Q. B. Chen, N. Kaiser, and U.-G. Meißner, *Eur. Phys. J. A* **57**, 161 (2021).
- [55] P.-W. Zhao, Z.-P. Li, J.-M. Yao, and J. Meng, *Phys. Rev. C* **82**, 054319 (2010).
- [56] W. Urban, J. Durell, A. Smith, W. Phillips, M. Jones, B. Varley, T. Rzaca-Urban, I. Ahmad, L. Morss, M. Bentaleb *et al.*, *Nucl. Phys. A* **689**, 605 (2001).
- [57] S. Frauendorf and F. Dönau, *Phys. Rev. C* **92**, 064306 (2015).
- [58] Y. R. Shimizu and M. Matsuzaki, *Nucl. Phys. A* **588**, 559 (1995).
- [59] F. Q. Chen, Q. B. Chen, Y. A. Luo, J. Meng, and S. Q. Zhang, *Phys. Rev. C* **96**, 051303(R) (2017).